PSFC/JA-01-11

17 GHz PHOTONIC BAND GAP CAVITY WITH IMPROVED INPUT COUPLING

Shapiro M.A., Brown W.J., Mastovsky I.,
Sirigiri J.R., and Temkin R.J.

June 2001

Plasma Science and Fusion Center
Massachusetts Institute of Technology
Cambridge, MA 02139, USA

This work was supported by the U.S. Department of Energy under the High Energy Physics program.

Published in *Physical Review Special Topics – Accelerators and Beams*, Vol. **4**, 042001 (2001).

17 GHz PHOTONIC BAND GAP CAVITY WITH IMPROVED INPUT COUPLING

M. A. Shapiro, W. J. Brown, I. Mastovsky, J. R. Sirigiri, and R. J. Temkin
Plasma Science and Fusion Center,
Massachusetts Institute of Technology,
167 Albany Street, Cambridge, MA 02139
Internet: shapiro@psfc.mit.edu, http://www.psfc.mit.edu/wab/

(Dated: May 10, 2001)

We present the theoretical design and cold test of a 17 GHz Photonic Band Gap (PBG) cavity with improved coupling from an external rectangular waveguide. The PBG cavity is made of a triangular lattice of metal rods with a defect (missing rod) in the center. The TM_{010} - like defect mode was chosen as the operating mode. Experimental results are presented demonstrating that critical coupling into the cavity can be achieved by partial withdrawal or removal of some rods from the lattice, a result that agrees with simulations. A detailed design of the PBG accelerator structure is compared with a conventional (pillbox) cavity. One advantage of the PBG cavity is that its resonance frequency is much less perturbed by the input/output coupling structure than in a comparable pillbox cavity. The PBG structure is attractive for future accelerator applications.

PACS numbers: 84.40.Dc, 29.17.+w

I. INTRODUCTION

Photonic Band Gap (PBG) structures (photonic crystals) [1],[2], typically, built of periodic metallic and/or dielectric lattices, show tremendous potential for applications in guided wave optics — a field that employs the methods and techniques of microwave periodic structures for confinement, transmission and transformation of coherent optical radiation. The recent past has also witnessed significant research on theoretical and experimental modeling of PBG structures at microwave frequencies [3]–[5]. Furthermore, PBG components attract interest for traditional microwave applications because they can be built oversized (quasi-optical) and therefore, employed at higher frequencies and higher power.

A cavity made of a 2D PBG structure of metal rods has been proposed as a candidate for an accelerator cell [6]–[8]. The advantage of the PBG accelerating cavity lies in the efficient suppression of the higher-frequency, higher-order mode wakefields without affecting the operating mode [9],[10].

In this work, the operating frequency is chosen to facilitate future work on the MIT 17 GHz rf photocathode gun [11] and the 17 GHz linear accelerator currently operating at MIT in collaboration with Haimson Research Corporation [12]. The design and cold testing of this PBG cavity is the initial step in the demonstration of the merit of PBG cavities for high gradient accelerators. The 17 GHz PBG cavity was designed using the SUPERFISH code [13], which is a 2D eigenmode solver. This cavity is built of metal rods in the form of a triangular lattice. The PBG cavity design is described in Sec. II A.

The PBG cavity was cold tested using a vector network analyzer. The cavity was excited through the aperture of a rectangular waveguide. The cold test was modeled using the 3D HFSS simulator [14], and the results of the modeling were compared to the measurements. In the cold testing, we focused on the problem of coupling into the PBG cavity, a critical issue for accelerator applications. In a conventional pillbox cavity, the coupling can be adjusted only by changing the dimension of the coupling hole. However, coupling into a PBG cavity can be adjusted when the rods of the lattice are removed or partially withdrawn — a feature unique to PBG structures. A variety of coupling schemes are tested experimentally and the Q-factor of the PBG cavity for each of these schemes is measured. The cold test results and their comparison to the HFSS modeling is presented in Sec. II B.

The PBG cavity based accelerator cell including the beam holes is analyzed using the HFSS code. These results are presented in Sec. II C. This is followed by Discussion and Conclusions in Sec. III.

II. PBG CAVITY

A PBG CAVITY DESIGN

An experimental cold test cavity has been designed. A triangular lattice of metal rods with a defect (a missing rod at the center) forms the PBG cavity (Fig. 1). Since only a finite number of circular rows of rods are required to localize the defect mode, only three rows of rods were used in this case. The array of metal rods is held inside a metallic cylinder closed on both ends. The operating

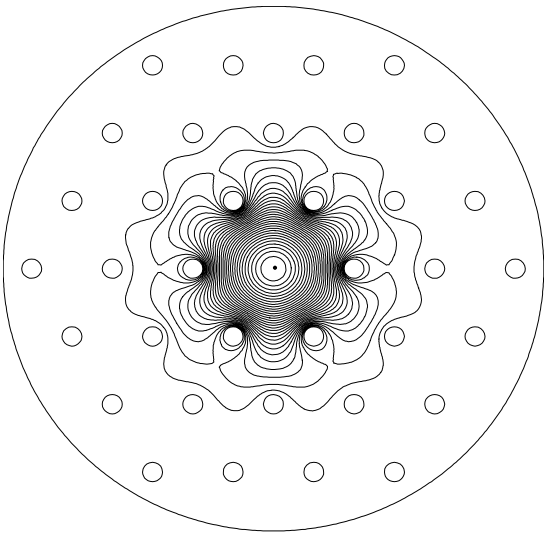

FIG. 1: Cross-section of the PBG cavity geometry. The cavity is formed by metal rod lattice with a defect in the center and is surrounded by a metal wall. The contours of constant E-field are also plotted.

Parameter	**PBG Cavity**	**Pillbox Cavity**
Lattice vector	0.64 cm	
Rod radius	0.079 cm	
Cavity radius	2.15 cm	0.657 cm
Eigenfrequency	17.32 GHz (SF)	17.46 GHz (SF)
Cavity Length	0.787 cm	0.787 cm
Effective Rad.	0.388 cm	0.657 cm
Ohmic Q	5200	7100
Shunt Imped.	2.1 (MΩ/cm)	2.9 (MΩ/cm)
Coup. Freq.	17.32 GHz (SF) 17.25 GHz (HFSS)	17.16 GHz (SF) 17.20 GHz (HFSS)
$H_{\max} Z_0/E_{\max}$	1.3 (SF)	0.94 (SF)

TABLE I: PBG cavity and equivalent pillbox cavity parameters.

mode for the cavity is chosen to be a quasi-TM_{010} defect mode. In such a mode the electric field is parallel to the rods, and the magnetic field is in the plane of the drawing.

The SUPERFISH code [13] is employed to calculate the eigenmodes and eigenfrequencies of both the PBG cavity and an equivalent pillbox cavity. The dimensions and simulation results are shown in Table I. The lines of constant electric field in the PBG cavity (the SUPERFISH output plot) are shown in Fig. 1. It is seen in Fig. 1 that the mode is localized in the vicinity of the defect. Near the axis, the mode is similar to the TM_{010} mode of a pillbox cavity. In the vicinity of the rods, the mode is no longer azimuthally symmetric and it extends to the third row of the rods. The comparison of the PBG cavity field structure with a pillbox cavity is discussed in detail in a later section.

The Q-factor of the PBG cavity is calculated using the field distribution obtained from SUPERFISH. The ohmic Q-factor of the cavity is expressed as follows:

$$Q_{ohm} = \frac{1}{d_{sk}\left(\frac{1}{R_{eff}} + \frac{1}{L_{\|}}\right)}, \tag{1}$$

where the skin-layer depth d_{sk} =0.5 μm at 17 GHz, $L_{\|}$ is the axial length, and an effective radius of the mode, R_{eff}, is defined as

$$R_{eff} = 2\int_{S_\perp} H^2 dS_\perp \left(\oint_{l_i} H^2 dl\right)^{-1}. \tag{2}$$

In (2), the magnetic field H is integrated over the cavity cross-section $S_\perp$ and over all contours l_i of the rods. The stored energy per unit axial length is computed by SUPERFISH using

$$W = \frac{\mu_0}{2}\int_{S_\perp} H^2 dS_\perp, \tag{3}$$

where μ_0(=$4\pi\times10^{-7}$Henry/m) is the permeability of vacuum. It may be mentioned that R_{eff} is equal to the cavity radius R for a pillbox cavity. A specific shunt impedance is expressed as follows

$$r_{cy} = \frac{E_{\max}^2}{\omega W} Q_{ohm}, \tag{4}$$

where $E_{\max}$ is the peak axial electric field. The results of calculation of the effective radii, ohmic Q-factors, and shunt impedances are shown in Table I for the PBG cavity and the pillbox cavity. The somewhat higher values of the Q-factor and the shunt impedance of the pillbox cavity as compared to the PBG cavity can be attributed to the enhanced magnetic field at the location of the rods in the latter, leading to somewhat greater ohmic losses. A PBG cavity with thicker rods will have a higher value of both Q and r_{cy}.

We have analyzed the coupling to the PBG cavity from a WR62 rectangular waveguide operating at the fundamental TE_{10} mode. The width of the wide wall of the waveguide is 1.575 cm, while the narrow wall size is 0.788 cm which is equal to the height of the PBG cavity. The schematic of the waveguide coupling into the PBG cavity is shown in Fig. 2, the plot produced by HFSS. The TE_{10} mode (the electric field is along the narrow wall) couples into the PBG cavity through the rows of rods. We excite the cavity from the waveguide on the right of the cavity and a similar dummy waveguide is used on the left side of the cavity to symmetrize the fields. Two rods are removed from each side of the PBG cavity contiguous to the waveguide apertures. There is no coupling hole at the waveguide aperture, in contrast to a pillbox cavity in which the coupling is provided through the hole in the aperture of the waveguide.

The SUPERFISH code is employed to calculate the frequency shift caused by the coupling into the PBG cavity as well as into the pillbox cavity. The SUPERFISH

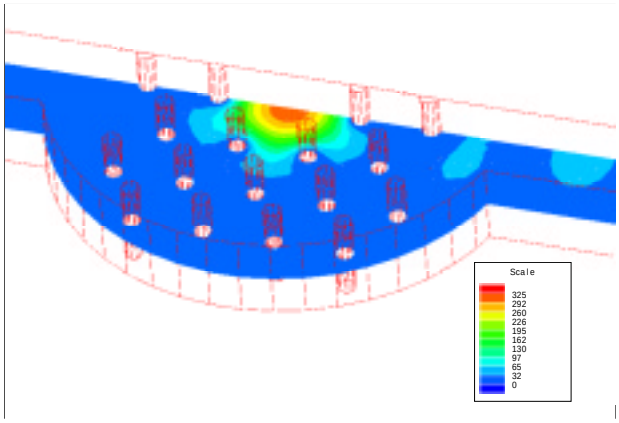

FIG. 2: The HFSS model of the PBG cavity and the waveguide coupling unit showing the magnitude of the electric field. The WR62 waveguide on the right is used for coupling the rf power into the cavity and a similar waveguide is used on the left to symmetrize the system. The PBG cavity and the waveguides are cut along the plane of symmetry which is specified as an H-wall in the simulations.

results are then checked using the HFSS code (see Sec. II B). In the pillbox cavity under comparison, the iris (coupling hole) is used. The dimensions of this iris are chosen such that the ratio of the axial field to the waveguide field in both PBG and pillbox cavities is the same in the SUPERFISH simulations. In the pillbox cavity, the iris goes all the way through the aperture. Its dimensions are the following: the width is 0.37 cm measured along the wide wall, and the depth is 0.2 cm measured along the waveguide. The coupling frequency and the eigenfrequency are determined by computing the resonance frequency with and without the coupling unit, respectively. The waveguide apertures are defined as magnetic walls in SUPERFISH to enable the computation of the frequency of the cavity with the coupling unit. The SUPERFISH calculation indicates that the coupling caused a 2 % frequency down-shift for the pillbox cavity, whereas there is no frequency shift caused by the coupling in the PBG cavity (Table I). The reason for this effect is the phenomenon of distributed coupling in a PBG cavity. In a PBG cavity the fields are confined by the first few rows of rods closest to the defect. These rods need not be disturbed for achieving coupling into the cavity and hence, coupling does not cause variations in the field pattern thus preserving the form of the original eigenmode.

In SUPERFISH simulations, we observe the magnetic field enhancement at the rods of the first row in the PBG cavity as well as at the edge of the iris in the pillbox cavity. The magnetic field enhancement is determined by the factor $H_{max}Z_0/E_{max}$, where Z_0=377 Ω , the maximum electric field is at the axis, and the maximum magnetic field is at some point at the metal surface. In the PBG cavity, this factor is 35% larger than that in the pillbox cavity (Table I). However, this factor can be reduced if

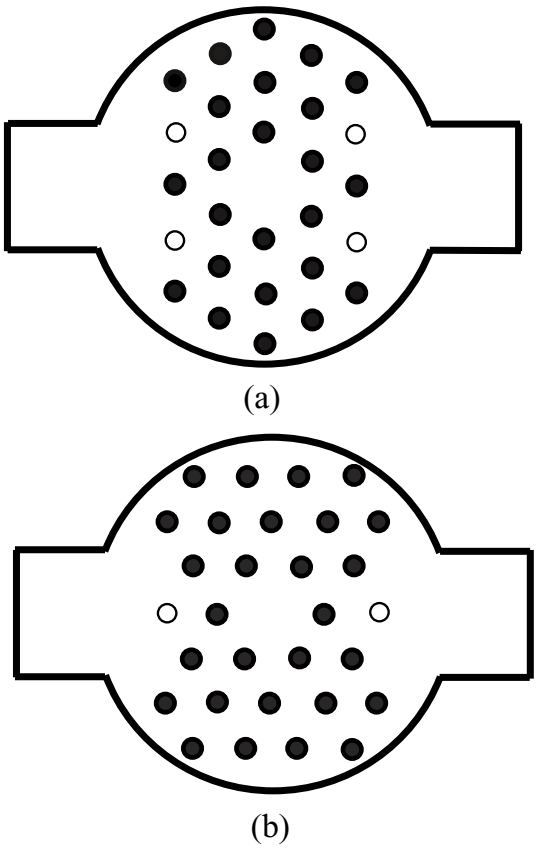

FIG. 3: (a) "Side" coupling scheme: partially withdrawn rods are shown as hollow circles while the rods shown as solid back dots form the actual cavity. (b) "Vertex" coupling scheme: partially withdrawn rods in green while the rods shown in red for m the actual cavity.

larger diameter rods are utilized.

B COLD TEST AND HFSS SIMULATIONS

A PBG cavity was fabricated using a brass cylinder closed at each end by a brass circular plate. The PBG structure was formed by thin copper rods fitted into an array of holes in the end plates. The rods were not brazed so as to facilitate their removal or insertion during cold tests. A WR62 rectangular waveguide was employed to feed rf power to the cavity. The same size waveguide was connected symmetrically to the opposite port. The PBG cavity dimensions are listed in Table I.

A vector network analyzer (VNA) was employed to experimentally characterize S_{11} and S_{12} elements of the scattering matrix. The measurements of the absolute value of S_{11} are presented in this paper; the S_{12} was also measured and demonstrated a typical resonance frequency dependence. The Smith chart measured by the VNA indicated that the cavity was undercoupled.

The six innermost rods surrounding the defect, the missing central rod, form a hexagon. Two orientations

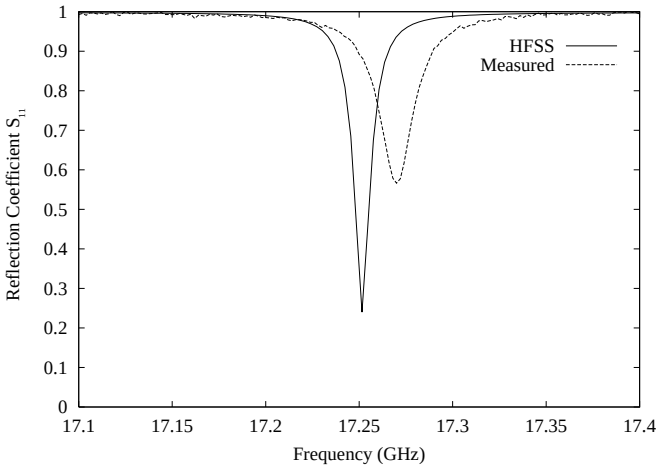

FIG. 4: "Vertex" coupling scheme with 6 rods removed: frequency dependence of the measured reflectivity, S_{11} (dotted line) and HFSS simulations (solid line).

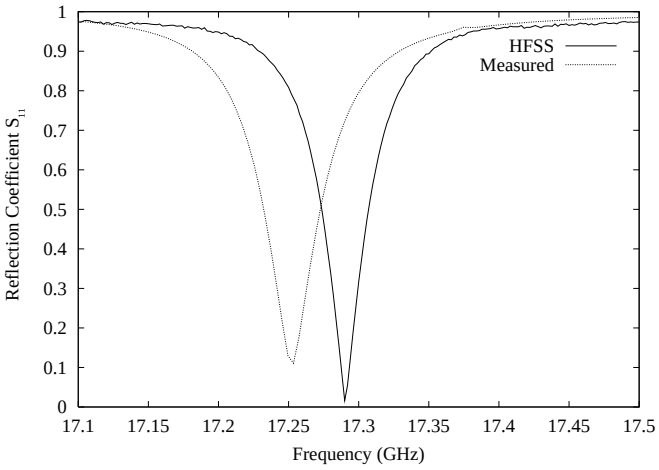

FIG. 5: "Vertex" coupling scheme with 6 rods removed and 2 rods partially withdrawn: frequency dependence of the measured reflectivity, S_{11} (dotted line) and HFSS simulations (solid line).

of the waveguide ports with respect to this hexagon have been studied in the present work. They are

1. rf power is coupled from the waveguide to the cavity through the side of the hexagon, as shown in Fig. 3(a) ("side" coupling)

2. rf power is coupled through the vertex of the hexagon ("vertex" coupling, Fig. 3(b)).

For coupling the rf power into the PBG cavity, rods are removed from the third row. In the scheme of "vertex" coupling (Fig. 3(b)), three rods are removed on the side of each port. The 3D electromagnetic code HFSS [14] was utilized to model the experiment. A cross-section of the 3D electric field profile predicted by HFSS simulations for the "vertex coupling scheme" is shown in Fig. 2. Taking advantage of the symmetry in the PBG cavity only a quarter of the cavity was modeled in HFSS simulations. The TE_{10} mode of a rectangular waveguide is incident from the right in Fig. 2. The waveguide mode couples very well into the PBG cavity forming a symmetrical electric field in the center of the cavity. The small reflection from the cavity formed a standing wave with a very low intensity as depicted in the waveguide section of the model in Fig. 2. The measured S_{11} frequency dependence (Fig. 4) indicates that the resonance frequency is 17.27 GHz for the "vertex" coupling scheme. It is 50 MHz lower than that predicted by SUPERFISH (Table I).

HFSS simulations were used to compute the frequency dependence of S_{11} (S_{12}) while including the ohmic losses in the cavity. In these simulations, the cavity walls and the rods are assumed to be made of copper (σ=5.8×10^7 Siemens/m). From the Smith chart representation of S_{11} produced by HFSS, it was found that the PBG cavity was undercoupled. This agrees with the cold test measurements. The S_{11} curve predicted by HFSS is plotted in Fig. 4 and shows the resonance frequency to be 17.25 GHz. The experimentally measured and HFSS predicted resonance frequencies are very close, the 0.2% difference in these frequencies can be attributed to a 0.001 normalized error in the rod radius.

Coupling Scheme	Meas. Q_{loaded}	Meas. Q_{ohmic}	HFSS Q_{loaded}	HFSS Q_{ohmic}
Vertex, 6 ⊗	700	900	1200	1900
Side, 8 ⊗	800	1000	1400	2100
Vertex, 6 ⊗ and 2 ⊘	300	600	250	500
Side, 8 ⊗ and 4 ⊘	300	600	130	250

TABLE II: Measured and HFSS simulated Q-factors for different coupling schemes. ⊗ are missing rods and ⊘ are the partially withdrawn rods.

It is evident from Table I that the HFSS calculated coupling frequencies are not exactly equal to the SUPERFISH results. The 3D HFSS simulations model the coupling into the PBG cavity better than the 2D simulations of SUPERFISH. The SUPERFISH code is faster and hence a wise choice for the preliminary design of the cavity while HFSS simulations are used for optimizing the design.

The loaded and ohmic Q-factors of the PBG cavity are calculated from the S_{11} curve. Since the cavity is undercoupled, the coupling coefficient β is related to the minimum S_{11} value as by $\beta = (1 - S_{11\,\mathrm{min}})/(1 + S_{11\,\mathrm{min}})$. The loaded Q-factor $Q_L = f/\Delta f$ can be determined from the frequency curve width Δf at the level where $S_{11\Delta f} = (1 + \beta^2)^{1/2}/(1 + \beta)$. The ohmic Q-factor is $Q_0 = (1 + \beta)Q_L$.

The experimentally measured and theoretically predicted values of the Q-factors are listed in Table II. It is seen that the experimentally measured Q-factor is half of the value predicted by HFSS. This difference can be attributed to the additional losses in the experimental

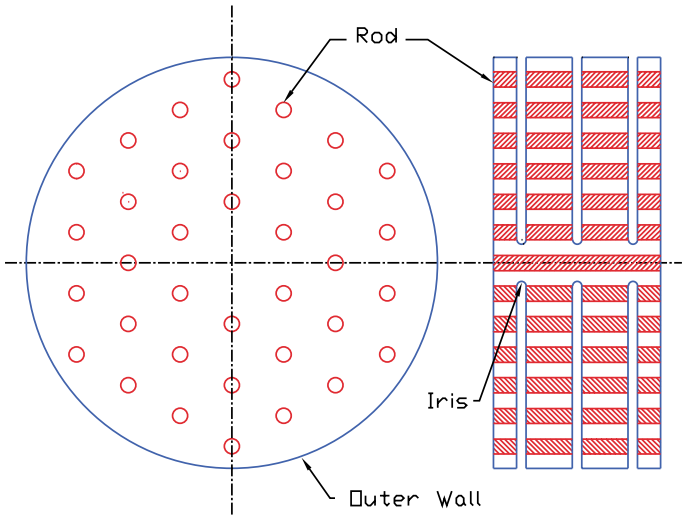

FIG. 6: The transverse and axial cross-sections of the PBG accelerator $2\pi/3$ structure. The metal rods are set between the disks. The beam holes are formed of the irises in the disks. The iris dimensions are scaled from the SLAC design.

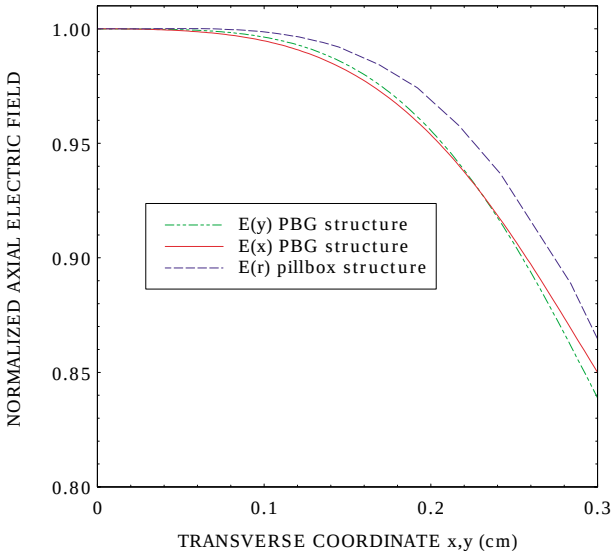

FIG. 7: Transverse accelerating field distributions near the axis in the $2\pi/3$ PBG and pillbox structures.

structure due to imperfect electrical contact between the rods and the entire structure. The rods are not brazed to the structure to allow flexibility in the partial withdrawal of rods to optimize coupling.

The "side" coupling scheme (four rods are removed, Fig. 3(a)) demonstrated similar performance to the "vertex" scheme (see Table II). Hence in both"vertex" and "side" schemes of coupling, the PBG cavity is undercoupled. By partial withdrawal of some of the rods from the lattice one may tune the coupling. In the present case this is done by the partial withdrawal of the rods from the second row. With the cavity set in the "vertex" position (Fig. 3(b)), critical coupling was achieved with this correction procedure, as shown in Fig. 5. This effect is confirmed by the HFSS simulations, also shown in Fig. 5. The coupling coefficient β becomes almost unity at critical coupling; therefore, the loaded Q-factor can be estimated to be half of the ohmic Q-factor.

Coupling correction is also possible if the "side" coupling scheme is in use. To reach critical coupling, two rods were partially withdrawn on each side of the cavity, as shown in Fig. 3(a). This procedure was modeled in HFSS by withdrawing four rods symmetrically half way through the cavity. The measurement and simulation results for this scheme are listed in Table II. The coupling correction indicated a noticeable increase in the ohmic losses due to the electric field enhancement at the ends of the partially withdrawn rods. Alternatively, instead of withdrawing the rods, the rods may be replaced by thinner rods fitted all the way through the cell. Such a method of coupling correction should not cause enhancement of ohmic losses.

C PBG ACCELERATOR CELL

A disk-loaded $2\pi/3$ accelerator structure can be built with a stack of PBG cavities set between the disks with the beam holes (irises) inserted on axis. Fig. 6 depicts the three cell structure that models the $2\pi/3$ structure. The irises are similar to those in a conventional linear accelerator consisting of pillbox cavities. The iris has a tip curvature radius equal to half of the thickness of the disk. The iris dimensions as well as the axial period of the PBG structure, are scaled by a factor of six from the SLAC 2.856 GHz accelerator design [15]. The rod spacing and diameter are the same as those in the cold test PBG cavity (Table I). The other parameters are listed in Table III.

The HFSS eigenmode solver was employed to determine the properties of the PBG accelerator structure with beam holes. Because of the symmetry of the $2\pi/3$ mode in the 3-cell structure depicted in Fig. 6, a 1-and-1/2-cell structure was analyzed. The ideal metal E-wall boundary conditions were specified on all surfaces. The HFSS eigenfrequency solver was employed to calculate the resonant frequencies of the 1-and-1/2-cell PBG structure as well as the PBG cell without the beam holes. The results of calculation listed in Table III indicate that the beam holes lead to a 0.44 GHz (2.6 %) eigenfrequency shift.

A 1-and-1/2-cell pillbox 17 GHz structure scaled from the 2.856 GHz SLAC structure was also simulated using the HFSS and SUPERFISH codes. The iris dimensions of this structure are listed in Table III, and the cell radius is 0.6883 cm. The axial field distributions determined in the PBG and pillbox structures are found to be similar.

From the point of view of beam dynamics, it is important to determine the transverse field distribution in the structure. As is well known for the pillbox structure, the

Structure period (cm)	0.583
Straight section length (cm)	0.487
Iris radius (cm)	0.194
Disk thickness (cm)	0.096
Iris tip radius (cm)	0.048
Eigenfreq. of PBG 1-1/2-cell structure (GHz)	17.71
Eigenfreq. of PBG cell without beam holes (GHz)	17.27

TABLE III: Parameters of PBG accelerator cell.

beam holes affect the transverse field distribution in the midplane, making the distribution wider as compared to the zeroth-order Bessel function field distribution of the pillbox cavity without beam holes [16]. In the PBG accelerator structure the same effect was observed. From the HFSS calculated 2D field distribution $E(x, y)$ of the axial component of the electric field simulated at the end plate ($z = 0$), we derive the horizontal $E(x, 0)$ and vertical $E(0, y)$ distributions. The x-axis corresponds to the horizontal axis in the left drawing of Fig. 6, whereas the y-axis corresponds to the vertical axis. There is a significant field asymmetry between the x and y distributions in the PBG structure near the rods. However, this asymmetry is greatly reduced near the axis. The variation of the longitudinal electric field for the PBG cavity and a corresponding pillbox cavity are plotted in Fig. 7. It is evident from Fig. 7 that in a PBG accelerator cavity a beam of radius 0.5 mm would have a gradient within 0.1% of the axial value, which is suitable for accelerator applications.

III. DISCUSSION AND CONCLUSIONS

A 17 GHz PBG cavity built of a triangular lattice of metal rods has been designed, built and cold tested on a vector network analyzer. The test was modeled using HFSS and good agreement was obtained.

One of the many advantages of the PBG cavity is the variety of coupling schemes that can be implemented. The coupling into the operating TM_{010} mode was studied in the cold test using the "side" and "vertex" coupling schemes for two orientations of the waveguide with respect to the PBG cavity. Higher-order dipole modes will require damping. This can also be done using output coupling with waveguides. Depending on the dipole mode polarization, either "side" coupling, "vertex" coupling, or both can be used.

The PBG cavity is undercoupled as per the initial design. However, the coupling is corrected when some rods are partially withdrawn. The reflectivity from the cavity is brought from 32% down to 1.5%. This experimentally observed coupling control indicates the possibility to reach critical coupling into the PBG cavity using thinner rods which are equivalent to the partially withdrawn rods but with reduced ohmic losses. The thinner rods can be optimized using HFSS simulations in a future PBG cell design.

It is demonstrated that the coupling in the PBG cavity results in a much smaller frequency shift (0.2%) than that in a conventional pillbox cavity (2%). The critical coupling into the PBG cavity is obtained with an additional frequency shift of only 20 MHz. This can be attributed to the distributed coupling over the perimeter in the PBG cavity in contrast to the localized coupling through small apertures in a conventional pillbox cavity, where the frequency shift comes from a field distribution deformation due to the coupling holes. Though an inherent sextupole field asymmetry does exist in a PBG cavity, it enjoys the advantage of no additional field asymmetry due to the coupling.

The Q-factor and the shunt impedance were calculated. The Q-factor of the PBG cavity was measured and was found to be half of the theoretically computed value. It is believed that a higher Q would be obtained in a brazed structure. Good agreement between the cold test and the HFSS simulations allows us to conclude that the optimization and design of the brazed PBG structure can be completed using HFSS.

The PBG accelerator $2\pi/3$ structure including the beam holes was modeled. The 1-and-1/2-cell structure was simulated using the HFSS code. The results from the PBG structure were compared to those from the pillbox structure, and similar accelerating field profiles were found. The frequency upshift was determined to be 2.6% for the $2\pi/3$ PBG structure due to the beam holes as opposed to the PBG cavity measured in the cold test. The midplane field distribution in the $2\pi/3$ structure was simulated and found flattened near the axis. This is consistent with the pillbox $2\pi/3$ structure simulation.

ACKNOWLEDGMENTS

This work was supported by Dept. of Energy, High Energy Physics Contract DE-FG02-91ER40648.

REFERENCES

[1] E.Yablonovitch, T.J.Gmitter and K.M.Leung, Phys. Rev. Lett., **67**, 2295 (1991).

[2] J.D.Joannopoulos, R.D.Meade and J.N.Winn, Photonic Crystals: Molding the Flow of Light (Princeton Univ. Press, Princeton, 1995).

[3] D.R.Smith, R.Dalichaouch, N.Kroll, S.Schultz, S.L.McCall and P.M.Platzman, JOSA-B, **10**, 314 (1993).

[4] E.Yablonovitch, T.J.Gmitter, R.D.Meade, A.M.Rappe, K.D.Brommer and J.D.Joannopoulos, Phys. Rev. Lett., **67**, 3380 (1991).

[5] E.Ozbay, E.Mitchel, G.Tuttle, R.Biswas, M.Sigalas and K.M.Ho, Appl. Phys. Lett., **64**, 2059 (1994).

[6] D.R.Smith, S.Schultz, N.Kroll, M.Sigalas, K.M.Ho and C.M.Soukoulis, Appl. Phys. Lett., **65**, 645 (1994).

[7] D.R.Smith, N.Kroll and S.Schultz, Advanced Accelerator Concepts, AIP Conference Proceedings **335** (AIP, New York, 1995), p. 761.

[8] D.R.Smith, Derun Li, D.C.Vier, N.Kroll and S.Schultz, Advanced Accelerator Concepts, AIP Conference Proceedings **398** (AIP, New York, 1997), p. 518.

[9] Derun Li, N.Kroll, D.R.Smith and S.Schultz, Advanced Accelerator Concepts, AIP Conference Proceedings **398** (AIP, New York, 1997), p. 528.

[10] N.Kroll, S.Schultz, D.R.Smith, and D.C.Vier, Proc. 1999 Particle Accelerator Conf. (IEEE, 1999), p. 830.

[11] W.J.Brown, S.Trotz, K.E.Kreischer, M.Pedrozzi, M.A.Shapiro and R.J.Temkin, Nuclear Instrum. Meth. Phys. Res. A, **425**, 441 (1999).

[12] J. Haimson and B. Mecklenburg, Proc. 1995 Particle Accelerator Conf. (IEEE, 1995), p. 755.

[13] J.H.Billen and L.M.Young, POISSON SUPERFISH, Los Alamos National Laboratory, Report LA-UR-96-1834, 1996.

[14] HFSS Manual, ANSOFT Corp., 1999.

[15] P.B. Wilson, Applications of High Power Microwaves, A.V. Gaponov-Grekhov and V.L. Granatstein, editors (Artech House, 1994), p. 229.

[16] J.Haimson, B.Mecklenburg, and E.L.Wright, Advanced Accelerator Concepts, AIP Conference Proceedings **398** (AIP, New York, 1997), p. 898.